

# Spatial Distribution Profiles of Emtricitabine, Tenofovir, Efavirenz, and Rilpivirine in Murine Tissues Following *In Vivo* Dosing Correlate with Their Safety Profiles in Humans

Herana Kamal Seneviratne, Allyson N. Hamlin, Carley J. S. Heck, and Namandjé N. Bumpus\*

Cite This: *ACS Pharmacol. Transl. Sci.* 2020, 3, 655–665

Read Online

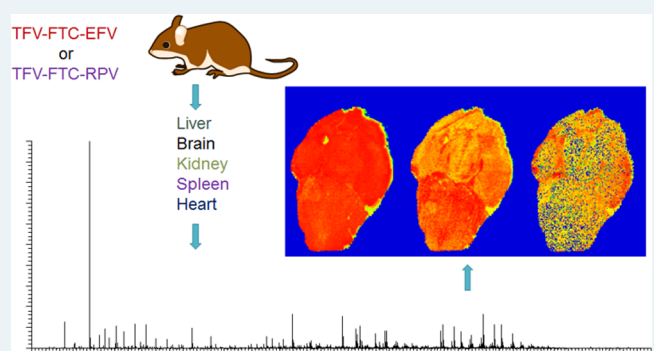
ACCESS |

Metrics & More

Article Recommendations

**ABSTRACT:** Emtricitabine (FTC), tenofovir (TFV), efavirenz (EFV), and rilpivirine (RPV) are currently used as components of HIV combination therapy. Although these drugs are widely used in antiretroviral therapy, several organ toxicities related to TFV and EFV have been observed clinically. TFV is associated with nephrotoxicity, whereas EFV-related hepatotoxicity and neurotoxicity have been reported. While the precise molecular mechanisms related to the above-mentioned clinically observed toxicities have yet to be elucidated, understanding the local tissue distribution profiles of these drugs could yield insights into their safety profiles. To date, the distributions of these drugs in tissue following *in vivo* exposure are poorly understood. Therefore, in this study, we employed a matrix-assisted laser desorption/ionization mass spectrometry imaging method to generate spatial distribution profiles of FTC, TFV, EFV, and RPV in mouse tissues following *in vivo* dosing of following drug regimens: TFV–FTC–EFV and TFV–FTC–RPV. For this study, liver, brain, kidney, spleen, and heart tissues were obtained from mice ( $n = 3$ ) following separate oral administration of the above-mentioned drug regimens. Interestingly, EFV was detected in liver, brain, and heart following TFV–FTC–EFV treatment. Additionally, hydroxylated EFV, which encompasses the cytochrome P450-dependent monooxygenated metabolites of EFV, was detected in liver, brain, spleen, and heart tissue sections. Notably, the tissue distribution profiles of RPV and hydroxylated RPV following *in vivo* dosing of TFV–FTC–RPV were different from EFV/hydroxylated EFV despite RPV belonging to the same drug class as EFV. In conclusion, the observed spatial distribution profiles of the study drugs are in agreement with their safety profiles in humans.

TFV-FTC-EFV or TFV-FTC-RPV



The diagram illustrates the experimental workflow. It starts with a mouse receiving treatment with either TFV-FTC-EFV or TFV-FTC-RPV. The organs of interest—Liver, Brain, Kidney, Spleen, and Heart—are then analyzed. This analysis produces mass spectrometry images (heatmaps) for each organ, showing the spatial distribution of the drugs. A chromatogram below the images shows the mass-to-charge ratio of the detected compounds.

**KEYWORDS:** tenofovir, emtricitabine, efavirenz, rilpivirine, mass spectrometry imaging, antiretrovirals

Emtricitabine (FTC), a deoxycytidine nucleoside analog reverse transcriptase inhibitor and tenofovir (TFV; prescribed as the tenofovir disoproxil fumarate prodrug), an acyclic nucleotide analog reverse transcriptase inhibitor, are currently used for HIV treatment and prevention.<sup>1–3</sup> Efavirenz (EFV) and rilpivirine (RPV), first- and a second-generation non-nucleoside reverse transcriptase inhibitors, respectively, are used for HIV treatment in combination with TFV and FTC.<sup>4,5</sup>

Although TFV, FTC, EFV, and RPV have widespread clinical use in antiretroviral therapy, the *in vivo* spatial distributions of these drugs in tissue, including those in which they are known to cause toxicity, have yet to be fully elucidated. Importantly, it has been reported that TFV is associated with kidney toxicity that leads to kidney injury (acute or chronic).<sup>6,7</sup> Similarly, EFV exerts central nervous system side effects including neurotoxicity.<sup>4,8–10</sup> Further, EFV-associated hepatotoxicity is observed clinically.<sup>11,12</sup> While the molecular mechanisms related to the above-mentioned

clinically observed toxicities have yet to be fully defined, understanding the spatial distribution patterns of these drugs could yield insight into their safety profiles.

It is known that HIV non-nucleoside reverse transcriptase inhibitors such as EFV and RPV are extensively metabolized by the cytochrome P450 superfamily of heme-containing monooxygenases. Specifically, EFV is primarily metabolized by cytochrome P450 2B6 whereas cytochrome P450 3A4 is involved in RPV primary metabolism.<sup>13,14</sup> Interestingly, a hydroxylated metabolite of EFV (EFV–OH) in which the oxygen is inserted at the 8-position has been associated with

Received: February 5, 2020

Published: April 23, 2020



both drug-induced neurotoxicity and hepatotoxicity.<sup>15,16</sup> In contrast, to date, there are no reports on the toxicities caused by hydroxylated metabolites of RPV (RPV-OH). However, the tissue distributions of EFV-OH and RPV-OH remain unknown.

It is reported that tissues such as brain and spleen can act as reservoirs for HIV that allow the persistence of HIV replication despite antiretroviral therapy.<sup>17–20</sup> Notably, poor penetration of antiretrovirals into certain tissues may facilitate the formation and existence of these reservoirs.<sup>21</sup> However, data on antiretroviral distribution across brain and spleen tissue are lacking. Therefore, there is a need to define the spatial distributions of antiretrovirals in HIV tissue reservoirs such as brain and spleen.

In previous studies, liquid chromatography–mass spectrometry (LC-MS) techniques have been employed to obtain tissue drug and/or metabolite concentrations.<sup>22</sup> For these analyses, homogenates from tissues or cell types isolated from tissues were utilized. However, using this approach, the spatial information on analytes is lost during sample preparation.<sup>23</sup> Because of this, it is impossible to determine the spatial distribution of drugs in tissue by employing LC-MS alone. In contrast, matrix-assisted laser desorption/ionization mass spectrometry imaging (MALDI MSI) bestows a powerful technology to visualize distribution profiles of a range of biomolecules including drugs, metabolites, peptides, proteins, and lipids from tissue slices.<sup>24,25</sup> Since MALDI MSI generates two-dimensional distribution profiles for each measured mass-to-charge ( $m/z$ ) ratio simultaneously, it yields greater specificity than other conventional imaging modalities such as fluorescence microscopy and autoradiography.<sup>25,26</sup> Of importance, high-resolution mass spectrometers such as orbitraps allow separation of analyte-specific peaks from other species such as background compounds that have similar masses, thereby increasing the veracity of identification.<sup>27</sup>

In this study, we employed a MALDI MSI strategy to visualize the distribution of TFV, FTC, EFV, and RPV in murine liver, brain, kidney, spleen, and heart tissues separately following *in vivo* dosing of drug regimens TFV–FTC–EFV and TFV–FTC–RPV. The observed tissue distribution patterns of the above drug molecules, TFV, FTC, EFV, and RPV in tissues were in agreement with their reported safety profiles. Furthermore, our MALDI MSI methodology enabled the visualization of distribution patterns of cytochrome P450-dependent monooxygenated metabolites of EFV and RPV, EFV-OH and RPV-OH. In sum, these results provide a unique foundation for understanding the tissue disposition of TFV, FTC, EFV, and RPV.

## METHODS

**Materials and Chemicals.** MALDI matrices, 2,5-dihydroxybenzoic acid (DHB),  $\alpha$ -cyano-4-hydroxycinnamic acid (CHCA), 1,5-diaminonaphthalene (DAN), and 9-aminoacridine (9-AA) were purchased from MilliporeSigma (St. Louis, MO). EFV and RPV were obtained through the National Institutes of Health AIDS Research and Reference Reagent Program (Germantown, MD), whereas TFV and FTC were purchased from Toronto Research Chemicals, Inc., (North York, ON, Canada). Drug tablets, TDF (tenofovir disoproxil fumarate)–FTC–EFV and TDF–FTC–RPV were obtained from the Johns Hopkins Hospital pharmacy. Other chemicals used and all solvents were either reagent- or high-performance liquid chromatography (HPLC)-grade and

obtained from Fisher Scientific (Hampton, NH), unless otherwise specified.

**MALDI Mass Spectrometry Analyses for Analyte Detection.** MALDI MS experiments were carried out in positive ion mode using an LTQ Orbitrap XL (Thermo Fisher Scientific, Bremen, Germany). This instrument was equipped with a Fourier transform mass spectrometer (FTMS) and the MALDI ion source fitted with a direct beam N<sub>2</sub> laser ( $\lambda = 337.7$  nm). Mass range used for data acquisition was from  $m/z$  100 to 1000 Da to cover the  $m/z$  values of TFV, FTC, EFV, and RPV. Mass spectrometry data processing and analysis were carried out using Xcalibur 3.0 (Thermo Fisher Scientific, Bremen, Germany).

### Tissue Sample Collection for MALDI MSI Analyses.

Animal model experiments were performed in accordance with Johns Hopkins Medicine Institutional Review Board guidelines and regulations. All mice (male and female, 8 week old C57BL/6J) were obtained from Jackson Laboratories (Bar Harbor, ME) and were administered drug regimens orally at doses of 70 mg/kg TFV–FTC–EFV and 33.4 mg/kg TFV–FTC–RPV via their drinking water for 28 days. Mice were given access to water *ad libitum* and average weekly water consumption of 4 mice/cage was  $185.5 \pm 10.23$  mL. Control experiments were carried out by administering drug-free water orally (via their drinking water). Mice were sacrificed after each treatment, and liver, brain, kidney, spleen, and heart tissues were dissected, embedded in OCT (embedding medium for frozen tissue specimens to ensure optimal cutting temperature; Sakura Finetek, Inc., Torrance, CA), snap-frozen in dry ice/acetone, and stored at  $-80$  °C.

**Tissue Sectioning and Matrix Application.** Tissue sections from frozen brain, spleen, heart, liver, and kidney at 20  $\mu$ m thickness were obtained at  $-20$  °C using a Leica CM3050S cryostat (Leica Biosystems, Buffalo Grove, IL). The sections were thaw-mounted onto glass microscope slides (Fisherbrand Superfrost Plus), and 10 mg/mL CHCA (Sigma-Aldrich, USA) in a mixture of ACN/H<sub>2</sub>O 50:50 (v/v) was applied to the tissue sections using a TM-Sprayer (HTX Technologies, LLC, Chapel Hill, NC) as described previously.<sup>28</sup>

### MALDI Mass Spectrometry Imaging of Mouse Tissue.

For drug-imaging experiments, regions of interest were defined by scanning the tissue sample slides with the MALDI camera. Distribution profiles of drugs were generated at a spatial resolution of 50  $\mu$ m. ImageQuest 1.1.0 software (Thermo Fisher Scientific, San Jose, CA) was used to generate ion images from imaging experiments. Ion suppression effects were determined by calculating tissue extinction coefficient (TEC) values for compounds of interest as described previously.<sup>28</sup> Briefly, TEC values of analytes were obtained by calculating the ratio of the relative ion abundance of analytes in tissue to their relative ion abundance when spotted directly onto a MALDI MS slide.

**H&E Staining.** Serial tissue sections were used for H&E staining to visualize the anatomy of tissue slices. Staining was done at the Oncology Tissue Services Laboratory, Johns Hopkins University School of Medicine using standard histological techniques.

## RESULTS

**MALDI MS Method Development for TFV, FTC, EFV, and RPV Detection.** The chemical structures of TFV, FTC, EFV, and RPV are shown in Figure 1. On the basis of previous

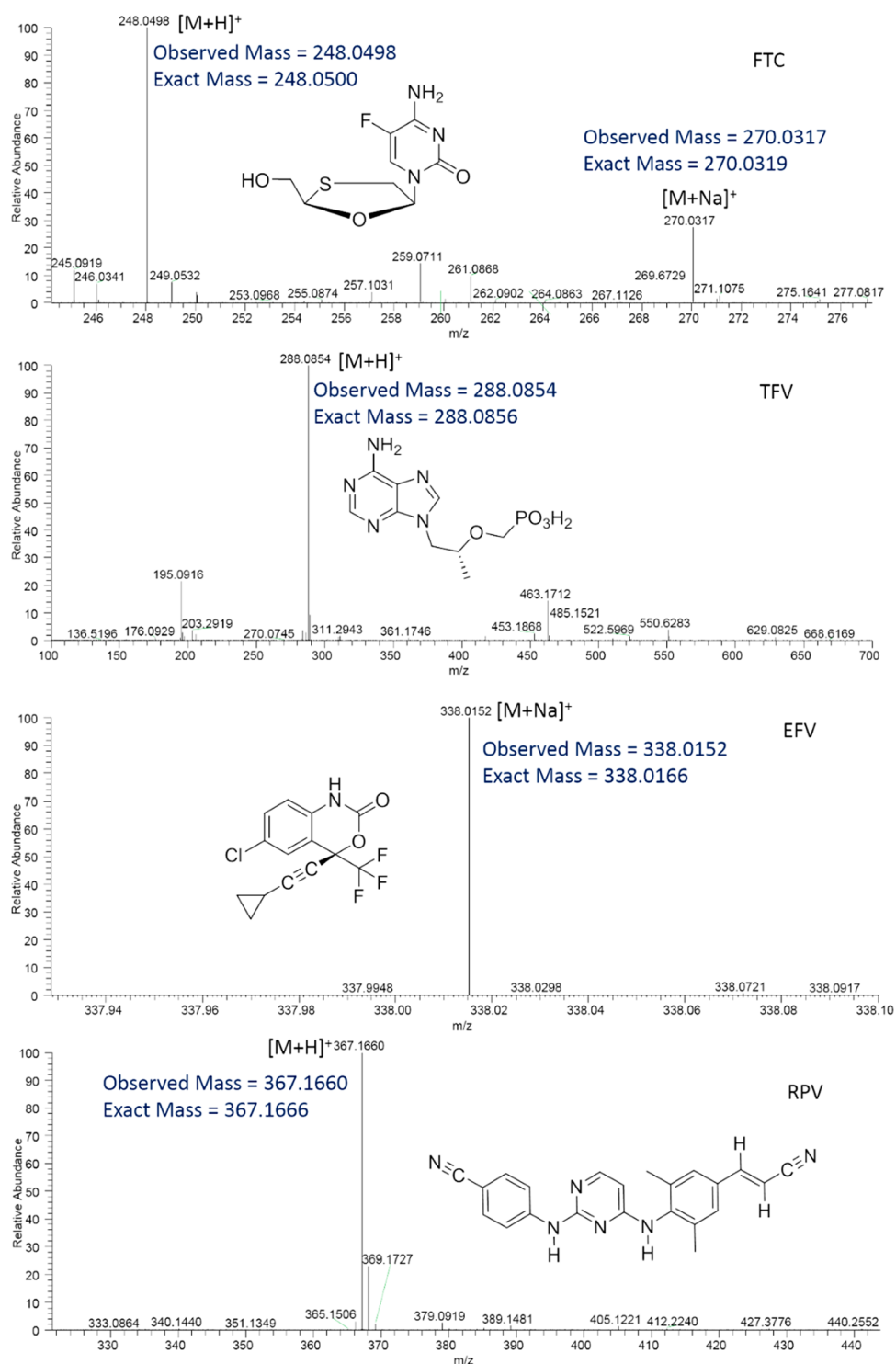


**Figure 1.** MALDI MS ionization of FTC, TFV, EFV, and RPV using the CHCA matrix and positive polarity of the instrument. Representative full scan mass spectra of FTC, TFV, EFV, and RPV exhibiting their detection. Drug molecules, FTC, TFV, EFV, and RPV were detected at  $m/z$  248.0498 (sodium adduct, 270.0317), 288.0854, 338.0152, and 367.1660, respectively.

reports on small-molecule MALDI MS, four different matrices, DHB, CHCA, DAN, and 9-AA, were employed to test the ionization efficiency of TFV, FTC, EFV, and RPV. Both DHB and CHCA facilitated the detection of all four compounds in the positive ion mode of the instrument. However, the signal intensity was greater with utilization of CHCA as compared to that with DHB. Therefore, CHCA was used as the matrix for subsequent experiments. From these, FTC, TFV, and RPV

exhibited their molecular ions at  $m/z$  248.0498 (0.8 ppm), 288.0854 (0.7 ppm), and 367.1660 (1.6 ppm), respectively, in positive ion mode (Figure 1). Additionally, sodium adducts of FTC and EFV were detected at  $m/z$  270.0317 (0.7 ppm) and 338.0152 (4.1 ppm), respectively (Figure 1). In order to further confirm the identities of the above molecules, collision-induced dissociation fragmentation was performed. From these analyses, FTC showed a major fragment ion at  $m/z$  130.0409

corresponding to the pyrimidine structural moiety,  $C_4H_5FN_3O^+$  (Table 1). Moreover, TFV, EFV, and RPV exhibited their fragment ions at  $m/z$  176.0927, 272.0429, and 224.1167 corresponding to  $C_8H_{10}N_5^+$ ,  $C_{13}H_{10}ClF_3N^+$ , and  $C_{14}H_{14}N_3^+$ , respectively (Table 1).

**Table 1. Confirmatory Collision-Induced Fragmentation Analyses of FTC, TFV, EFV, and RPV**

compound	mass fragment ( $m/z$ )	chemical formula
FTC	130.0409	$C_4H_5FN_3O^+$
TFV	176.0927	$C_8H_{10}N_5^+$
EFV	272.0429	$C_{13}H_{10}ClF_3N^+$
RPV	224.1169	$C_{14}H_{14}N_3^+$

**Spatial Distribution of TFV, FTC, EFV, and RPV in Mouse Liver Sections.** In order to determine the spatial distribution of TFV, FTC, and EFV in mouse liver tissues, MALDI MSI experiments were carried out using liver sections obtained from mice that received TFV–FTC–EFV. H&E stain was used to visualize the orientation and anatomy of the tissue section (Figure 2A). The spatial distribution profiles were generated using corresponding molecular ions and sodium

adducts of TFV, FTC, and EFV. All three drugs, TFV, FTC, and EFV, exhibited differential distribution across liver tissue sections (Figure 2A). Additionally, EFV–OH (the cytochrome P450-dependent monooxygenated metabolites of EFV collectively) was detected (Figure 2A). To further confirm that the observed differential distributions of TFV, FTC, EFV, and EFV–OH are distinct, we simultaneously imaged a known endogenous lipid species, phosphatidylcholine (PC) (16:0/OH). As expected, the MALDI MS ion images corresponding to PC (16:0/OH) exhibited relative homogeneity in their distribution (Figure 2A). Liver sections from mice treated with the drug regimen TFV–FTC–RPV were used to visualize RPV distribution. Interestingly, RPV was not accumulated in liver section following *in vivo* oral dosing of TFV–FTC–RPV via drinking water for 28 days, whereas hydroxylated RPV (RPV–OH) was readily detected (Figure 2B). Similar distribution patterns were observed for the localization of TFV, FTC, EFV, EFV–OH, and RPV in liver sections obtained from male mice following separate *in vivo* dosing of above drug regimens (Figure 2C,D). Notably, the relative abundance of RPV–OH in the tissue section obtained from male mice was lower compared to those of females (Figure 2D).

**Spatial Distribution of TFV, FTC, EFV, and RPV in Mouse Brain Sections.** Since brain is a highly heterogeneous

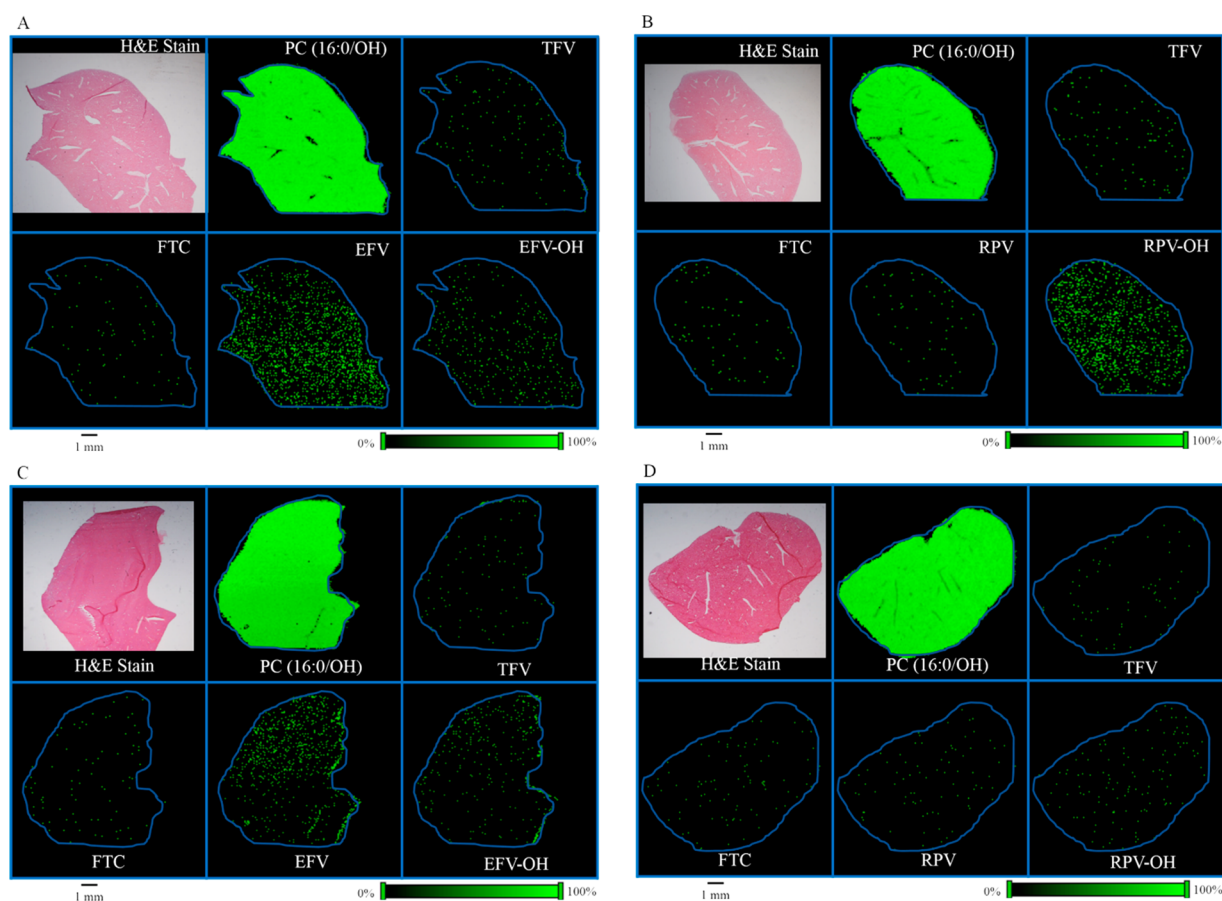


**Figure 2.** Spatial distribution of TFV, FTC, EFV, and RPV in mouse liver. Distribution profiles of PC (16:0/OH), TFV, FTC, EFV, and EFV–OH in liver sections of (A) female and (C) male mice following *in vivo* oral dosing of TFV–FTC–EFV. H&E stain indicating anatomy and orientation of liver tissue. Distribution profiles of PC (16:0/OH), TFV, FTC, RPV, and RPV–OH in liver sections obtained from (B) female and (D) male mice following *in vivo* oral dosing of TFV–FTC–RPV. Mice were administered drugs via their drinking water for 28 days and then sacrificed. MALDI MS ion images were generated at a spatial resolution of 50  $\mu$ m. The green color represents the highest signal intensity (100%), whereas the black color depicts the lowest signal (0%) of the ion of interest. Scale bar, 1 mm.

organ, we first generated the spatial distribution profile for the endogenous lipid species, PC (16:0/OH). As observed in the liver tissue sections, PC (16:0/OH) lipid species showed relative homogeneity in its distribution (Figure 3A). Additionally, we were able to detect endogenous creatine in brain sections using our MALDI MSI methodology and it was found to be relatively homogeneous across the brain tissue section (Figure 3A). Next, the spatial distributions of TFV, FTC, and EFV were visualized in brain sections of female mice dosed with TFV–FTC–EFV for 28 days via their drinking water. From these, TFV and FTC showed low abundance across the brain section (Figure 3A). However, the representative ion image of EFV revealed its heterogeneous distribution in the brain tissue (Figure 3A). Interestingly, EFV–OH was detected simultaneously in the same brain section (Figure 3A, lower panel). The distribution profiles of RPV and RPV–OH generated following *in vivo* dosing of TFV–FTC–RPV revealed the abundance of RPV–OH is greater than that of RPV in the mouse brain section (Figure 3B). We observed differential distribution of the above compounds in brain sections of male mice as well (Figure 3C,D).

**Spatial Distribution of TFV, FTC, EFV, and RPV in Mouse Kidney Sections.** In order to investigate the distribution of TFV, FTC, and EFV in kidney tissue, MALDI MS ion images corresponding to their molecular ions and sodium adducts were generated using kidney sections obtained from mice who received TFV–FTC–EFV. Ion images of endogenous lipid species, PC (16:0/OH), revealed its homogeneous distribution, whereas TFV and EFV exhibited heterogeneous distributions across the kidney tissue section (Figure 4A). In contrast, both FTC and EFV–OH were detected at low abundance (Figure 4A). To determine the spatial distribution of RPV and RPV–OH, kidney sections were obtained from mice dosed with TFV–FTC–RPV. Interestingly, RPV and RPV–OH did not accumulate in kidney sections (Figure 4B). Similar distribution patterns of all compounds were observed in male kidney sections (Figure 4C,D).

**Spatial Distribution of TFV, FTC, EFV, and RPV in Mouse Spleen Sections.** The spleen plays an important role in the immune system, and it can act as a tissue reservoir for HIV. Following *in vivo* dosing of TFV–FTC–EFV, the localization of EFV–OH in spleen sections were observed (Figure 5A). In contrast, mice that received TFV–FTC–RPV did not exhibit accumulation of RPV–OH (Figure 5B). The observed distribution patterns of all molecules were similar in male spleen sections (Figure 5C,D).

**Spatial Distribution of TFV, FTC, EFV, and RPV in Mouse Heart Sections.** Investigation of drug distribution in heart tissue is important to determine their potential cardiovascular effects. Therefore, in this study, mouse heart sections were obtained following separate TFV–FTC–EFV and TFV–FTC–RPV treatments. From MALDI MSI analysis, endogenous lipid species, PC (16:0/OH), and creatine exhibited relative homogeneity in their distribution across the heart section, whereas EFV and EFV–OH showed their heterogeneous distribution (Figure 6A). Notably, the relative abundances of EFV and EFV–OH were higher than TFV and FTC. To determine the spatial distribution of RPV and RPV–OH, heart tissue sections were obtained from mice treated with TFV–FTC–RPV for 28 days via their drinking water. From these, the accumulation of RPV and RPV–OH were not observed in heart sections (Figure 6B). As observed in female

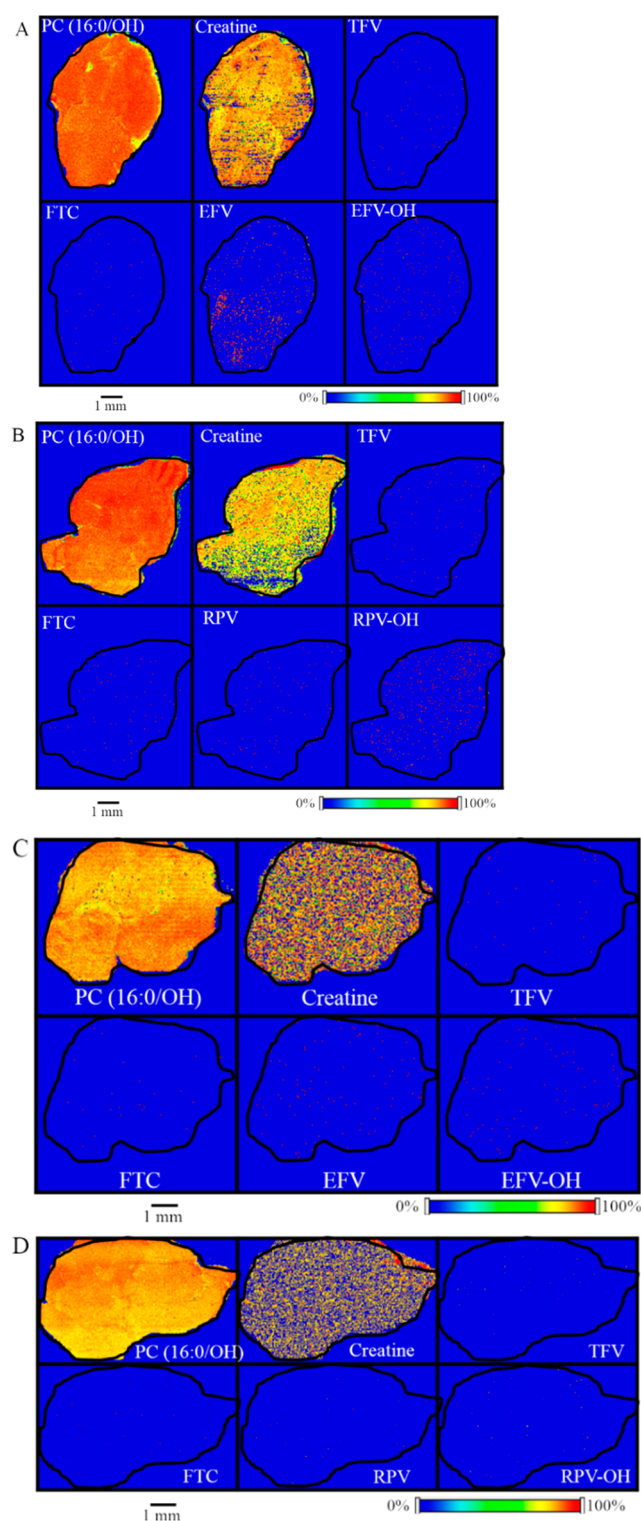


**Figure 3.** Spatial distribution of TFV, FTC, EFV, and RPV in mouse brain. Distribution profiles of PC (16:0/OH), creatine, TFV, FTC, EFV, and EFV–OH in brain sections obtained from (A) female and (C) male mice after *in vivo* dosing of TFV–FTC–EFV. Distribution profiles of PC (16:0/OH), creatine, TFV, FTC, RPV, and RPV–OH in brain sections of (B) female and (D) male mice following *in vivo* oral dosing of TFV–FTC–RPV. Mice were administered drugs via their drinking water for 28 days and then sacrificed. MALDI MS ion images were generated at a spatial resolution of 50  $\mu\text{m}$ . The red color represents the highest signal intensity (100%), whereas the blue color depicts the lowest signal (0%) of the ion of interest. Scale bar, 1 mm.

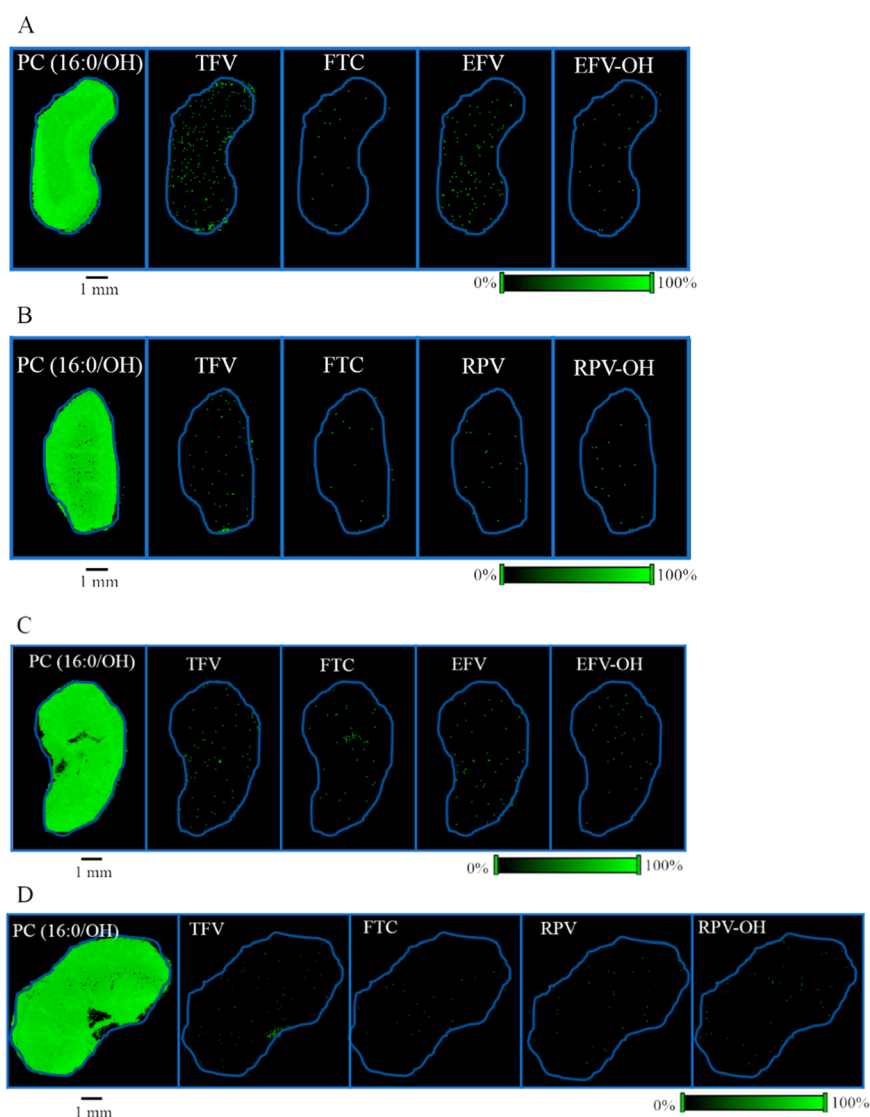


**Figure 4.** Spatial distribution of TFV, FTC, EFV, and RPV in mouse kidney. Distribution profiles of PC (16:0/OH), TFV, FTC, EFV, and EFV-OH in kidney sections obtained from (A) female and (C) male mice after *in vivo* dosing of TFV-FTC-EFV. Distribution profiles of PC (16:0/OH), TFV, FTC, RPV, and RPV-OH in kidney sections of (B) female and (D) male mice following *in vivo* oral dosing of TFV-FTC-RPV. Mice were administered drugs via their drinking water for 28 days and then sacrificed. Spatial resolution for MALDI MS ion images was 50  $\mu\text{m}$ . The green color represents the highest signal intensity (100%), whereas the black color depicts the lowest signal (0%) of the ion of interest. Scale bar, 1 mm.

heart sections, EFV and EFV-OH were accumulated in male heart sections, whereas RPV and RPV-OH were detected at low abundance (Figure 6C,D).

#### Values of $\log P$ and the Tissue Extinction Coefficient.

In order to calculate  $\log P$  values for TFV, FTC, EFV, and RPV, ALOGPS 2.1 software was used.<sup>29</sup> From these, the calculated  $\log P$  values of TFV, FTC, EFV, and RPV were  $-1.74$ ,  $-0.65$ ,  $4.15$ , and  $4.64$ , respectively (Table 2).

To study the effects on ionization of TFV, FTC, EFV, and RPV from endogenous substances in tissue, TEC values were determined. A mixture of above drugs was used to obtain the relative ion abundances of TFV, FTC, EFV, and RPV in blank tissue and directly on a MALDI MS slide. TEC values of TFV, FTC, EFV, and RPV are listed in Table 2.

## DISCUSSION

In the present study, the spatial distribution of TFV, FTC, EFV, and RPV in murine tissues was investigated using a

MALDI MSI strategy. All four drugs that were studied in this work are widely used to treat HIV infection. Monitoring the spatial distribution of drugs in tissue is important, mainly to determine their presence at target sites and to understand relevant toxicities due to accumulation. In addition to the visualization of the above-mentioned antiretrovirals, to our knowledge, this is the first study to image cytochrome P450 dependent monooxygenated metabolites of any antiretroviral in tissue following *in vivo* dosing.

On the basis of our data, we observed differential distribution of TFV, FTC, EFV, EFV-OH, RPV, and RPV-OH in liver tissue sections following *in vivo* dosing of TFV-FTC-EFV or TFV-FTC-RPV. Furthermore, using our MALDI MSI strategy, we were able to generate distribution maps of a range of endogenous molecules across tissue sections. Notably, we validated that the observed drug distribution profiles were distinct by demonstrating the relative homogeneous distribution of an endogenous lipid molecule,

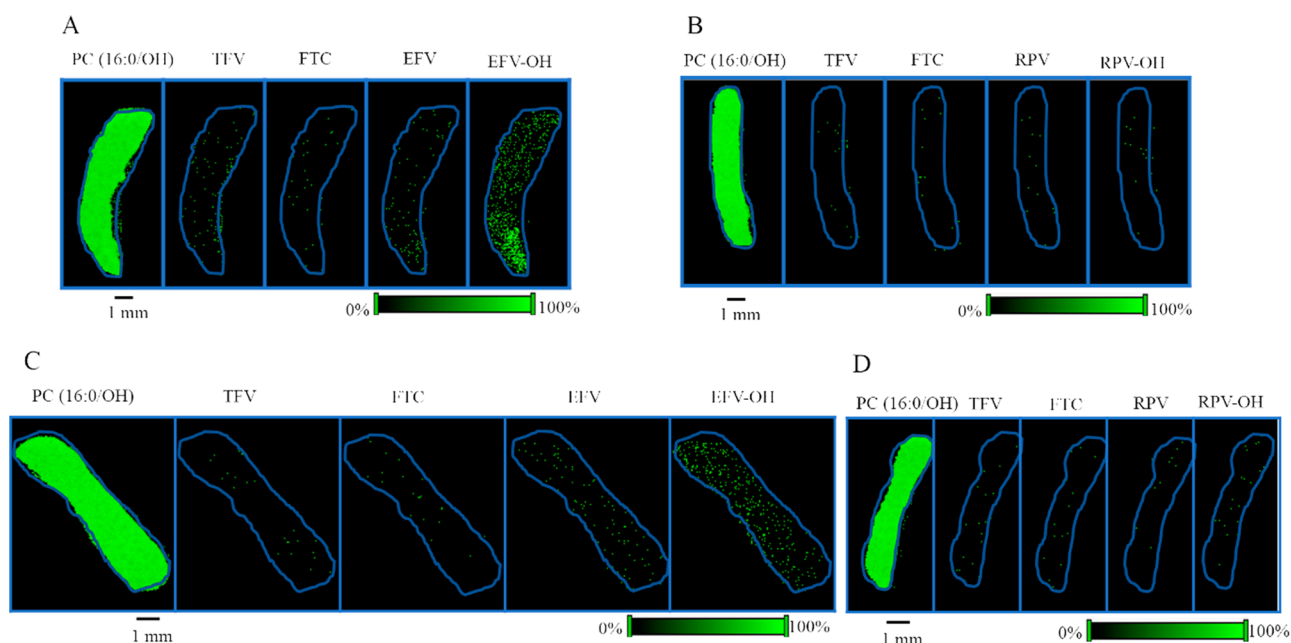


**Figure 5.** Spatial distribution of TFV, FTC, EFV, and RPV in mouse spleen. Distribution profiles of PC (16:0/OH), TFV, FTC, EFV, and EFV–OH in spleen sections obtained from (A) female and (C) male mice after *in vivo* dosing of TFV–FTC–EFV. Distribution profiles of PC (16:0/OH), TFV, FTC, RPV, and RPV–OH in spleen sections of (B) female and (D) male mice following *in vivo* oral dosing of TFV–FTC–RPV. Mice were administered drugs via their drinking water for 28 days and then sacrificed. Spatial resolution for MALDI MS ion images was 50  $\mu\text{m}$ . The green color represents the highest signal intensity (100%), whereas the black color depicts the lowest signal (0%) of the ion of interest. Scale bar, 1 mm.

PC (16:0/OH), simultaneously. It should also be noted that the heterogeneous distributions of endogenous metabolites could also be discerned, for instance, PC 30:0 and PC 40:7 (data not shown).

On the basis of two-dimensional drug distribution profiles in liver sections, the relative abundance of EFV was high compared to that in other organs. Of importance, EFV-associated hepatotoxicity has been observed clinically.<sup>30–32</sup> Conversely, hepatotoxicity is rare with TFV, and there are no reports of hepatotoxicity related to FTC.<sup>33,34</sup> Commensurate with this, we did not observe TFV and FTC in liver in high abundance. We did not observe the accumulation of RPV in liver tissue following *in vivo* dosing of TFV–FTC–RPV. Interestingly, it has been reported that RPV has a favorable safety profile as compared to that of EFV.<sup>35</sup> Thus, our findings are in concordance with previous literature on safety profiles of TFV, FTC, and EFV.

EFV is known to undergo hepatic metabolism to several metabolites, including mono- and dioxygenated metabolites formed by cytochrome P450 enzymes.<sup>36</sup> Cytochrome P450 2B6 is the major enzyme responsible for 8-hydroxylation of EFV, whereas cytochrome P450 2A6 is involved in EFV 7-hydroxylation.<sup>13,37</sup> While the molecular mechanisms related to EFV-associated hepatotoxicity are not fully elucidated, *in vitro* studies previously performed in our laboratory have suggested that the 8-hydroxy EFV metabolite may contribute to the observed toxicities.<sup>15</sup> Recent work in our laboratory by Heck et al. demonstrated the activation of hepatic cell stress regulators in the presence of EFV, inositol-requiring enzyme 1 $\alpha$  (IRE1 $\alpha$ ) and X-box-binding protein 1 (XBP1).<sup>38</sup> This IRE1 $\alpha$ –XBP1 activation may contribute to the cell death of hepatocytes by EFV. We detected EFV–OH in addition to EFV in liver sections, and similar to EFV, hydroxylated EFV exhibited heterogeneous distribution. It should be noted that EFV has

two hydroxylated metabolites, 7-hydroxy and 8-hydroxy EFV; therefore, a group of isomeric metabolites may be generated during the EFV metabolism. Due to the lack of liquid chromatography separation capabilities when using MALDI MSI, this approach is unable to distinguish hydroxylated isomeric compounds. Similarly, we detected RPV–OH in liver sections following *in vivo* dosing of TFV–FTC–RPV. Notably, the relative abundance of RPV–OH was higher than RPV. However, to date, the toxicity of RPV–OH has not been reported.

The mouse homologues of cytochrome P450 2B6 and 3A4 are cytochrome P450 2b10 and 3a11, respectively.<sup>39</sup> An apparent sex difference in RPV–OH distribution profiles in liver was observed. While the specific cytochrome P450s in mice responsible for RPV metabolism are unknown, several mouse cytochrome P450s exhibit sexually dimorphic expression. For example, the expression of murine cytochrome P450 3a41 and 3a44 in liver has been shown to be specific to female mice.<sup>40,41</sup> Previously, glucuronidated and sulfated forms of EFV hydroxylated metabolites have been detected in human plasma, urine, and cerebrospinal fluid (CSF), whereas glucuronidated forms of RPV hydroxylated metabolites have been reported from human plasma and urine.<sup>14,36,42</sup> However, *in vivo* conjugative metabolism of hydroxylated EFV and RPV in murine tissue has yet to be reported. In our study, we did not detect any conjugated metabolites of EFV–OH and RPV–OH.

EFV is associated with central nervous system disturbances, and EFV-induced neurotoxicities have been shown to have long-term effects.<sup>43</sup> Our MALDI MSI data revealed the heterogeneous distribution of EFV and EFV–OH in brain sections. Previously, the accumulation of EFV in brain tissue has been investigated using a physiologically based pharmacokinetic modeling approach.<sup>44</sup> Similarly, EFV accumulation in

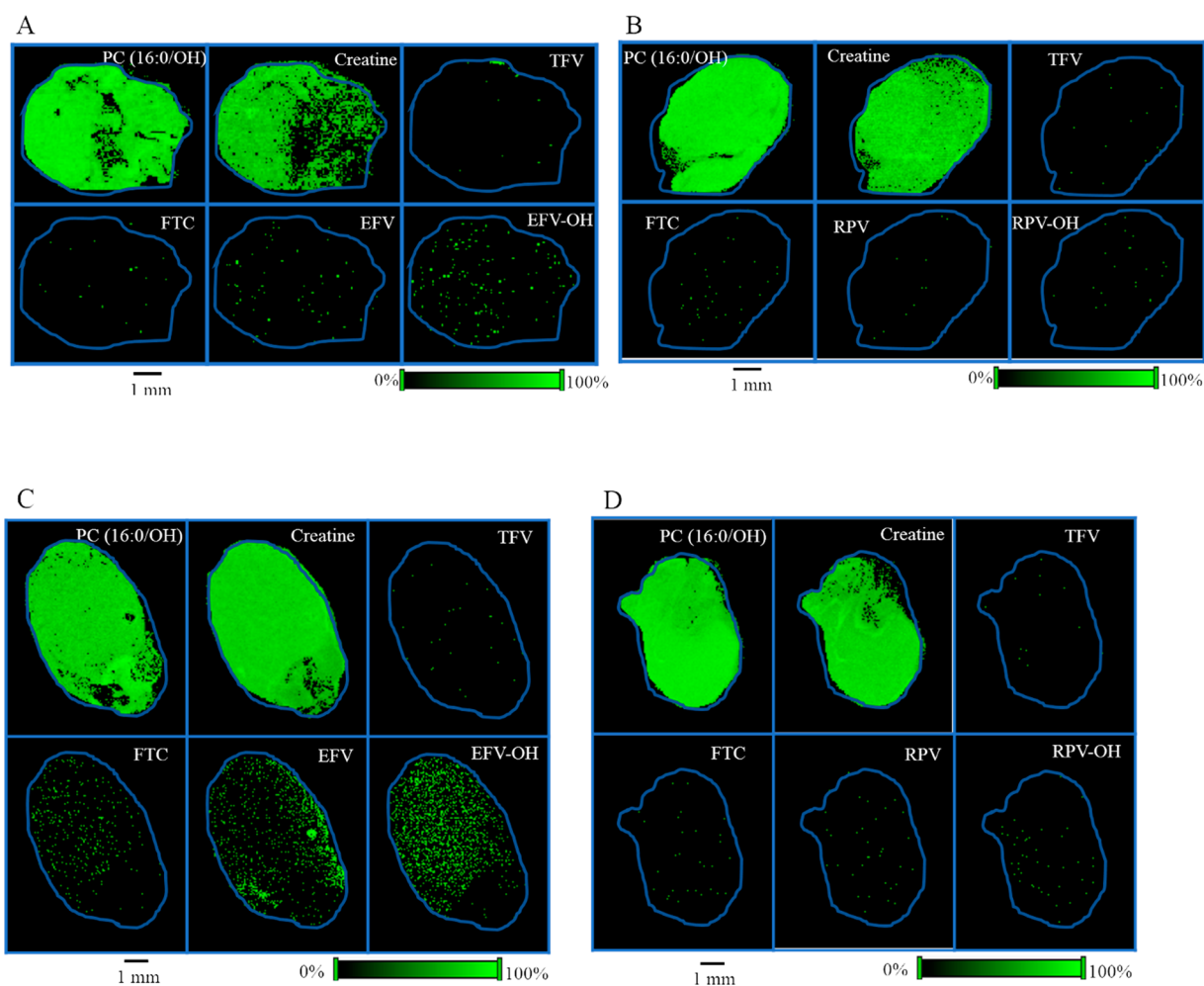


**Figure 6.** Spatial distribution of TFV, FTC, EFV, and RPV in mouse heart. Distribution profiles of PC (16:0/OH), creatine, TFV, FTC, EFV, and EFV-OH in heart sections obtained from (A) female and (C) male mice after *in vivo* dosing of TFV-FTC-EFV. Distribution profiles of PC (16:0/OH), creatine, TFV, FTC, RPV, and RPV-OH in heart sections of (B) female and (D) male mice following *in vivo* oral dosing of TFV-FTC-RPV. Mice were administered drugs via their drinking water for 28 days and then sacrificed. Spatial resolution for MALDI MS ion images was 50  $\mu\text{m}$ . The green color represents the highest signal intensity (100%), whereas the black color depicts the lowest signal (0%) of the ion of interest. Scale bar, 1 mm.

**Table 2.** Calculated TEC Values of TFV, FTC, EFV, and RPV for Murine Tissues (Liver, Brain, Kidney, Spleen, and Heart) and Predicted log *P* Values

compound	TEC in liver tissue	TEC in brain tissue	TEC in kidney tissue	TEC in spleen tissue	TEC in heart tissue	log <i>P</i> value
TFV	0.0769	0.0082	0.0097	0.0048	0.0110	-1.74
FTC	0.0401	0.0174	0.0017	0.0009	0.0061	-0.65
EFV	0.0358	0.1300	0.0045	0.0153	0.0319	4.15
RPV	0.0094	0.2377	0.0633	0.0436	0.0161	4.64

macaque brain tissue was reported.<sup>45</sup> Additionally, we were able to detect EFV-OH in brain tissues. Interestingly, *in vitro* neurotoxicity of the primary metabolite of EFV, 8-hydroxy EFV, has been demonstrated at concentrations similar to that in cerebrospinal fluid.<sup>16</sup> We detected RPV and RPV-OH in brain sections following *in vivo* dosing of TFV-FTC-RPV. Although there is no reported pharmacology/toxicology of RPV-OH, our data provides a motive to look at what these metabolites might be able to do in cells and tissues. While increased hydrophilicity by P450 metabolism is generally thought to facilitate rapid compound excretion from the body,

our data suggests that monooxygenated metabolites of EFV and RPV are present at detectable levels in tissues.

Notably, brain is known as an HIV tissue reservoir and is a target for HIV-1 infection. HIV-RNA and DNA have been detected in the brain tissue of subjects receiving antiretroviral therapy.<sup>18</sup> Low antiretroviral penetration is a reasonable explanation for the persistence of tissue HIV reservoirs. Antiretrovirals have varying abilities to cross the blood-brain barrier (BBB). Efflux transporters present in the BBB including P-glycoprotein may decrease the drug penetration into the brain.<sup>46</sup> Interestingly, it has been reported that EFV disrupts the integrity of the BBB resulting in an increase in permeability.<sup>47</sup> Although varying degrees of antiretroviral penetration into the brain have been reported, our MALDI MSI drug distribution data add to these existing findings by providing the spatial distributions of TFV, FTC, EFV, and RPV across brain tissue slices.

We observed the accumulation of TFV in mouse kidney tissue sections after *in vivo* dosing. Previously, accumulation of TFV in kidneys of rats that received radiolabeled TFV intravenously has been shown using positron emission tomography.<sup>48</sup> Kidney is a major organ responsible for drug



excretion. Interestingly, TFV-associated nephrotoxicity has been reported clinically.<sup>49–51</sup> It is known that TFV is actively transported into the proximal tubular cells of the kidney by organic anion transporters.<sup>52</sup> In addition, multidrug resistance proteins are involved in the efflux of TFV.<sup>53</sup> On the basis of previous work, the target site for TFV-related nephrotoxicity is the proximal tubule of the kidney.<sup>54</sup> MALDI MS images of TFV obtained at 50  $\mu\text{m}$  spatial resolution in kidney tissue sections further confirm the accumulation of TFV in kidney tissue by providing the spatial distribution patterns. Additionally, it would be interesting to examine the alterations of TFV distribution profiles in mouse kidney tissue by coadministering an inhibitor of multidrug resistance protein efflux transporters.

In order to further extend our work, we ascertained the distribution of above-mentioned drugs into spleen, also a known HIV tissue reservoir. Of importance, spleen is the largest secondary lymphoid organ, and it has an important role in the immune system as well as the circulatory system.<sup>20</sup> Investigations of antiretroviral distributions are rarely performed in spleen tissue, although the detection of both HIV RNA and DNA in spleen has been reported.<sup>20</sup> We observed the accumulation of EFV–OH in spleen sections following TFV–FTC–EFV treatment. This observation warrants further investigations of EFV disposition in spleen tissue.

It is known that certain classes of antiretrovirals can significantly contribute to cardiovascular abnormalities. In particular, EFV treatment is associated with an approximate 1.5-fold greater risk of adverse cardiovascular events as compared to patients not under antiretroviral therapy.<sup>55</sup> To date, there are no prior reports on antiretroviral distribution in heart tissue. From our study, we detected both EFV and EFV–OH in heart tissue following *in vivo* dosing of TFV–FTC–EFV.

Distribution of the above antiretrovirals may be driven by their physicochemical properties. Physicochemical properties that impact drug distribution include protein binding, molecular weight and lipophilicity ( $\log P$  value). Two nucleotide/nucleoside reverse transcriptase inhibitors, TFV and FTC, exhibit low protein binding (7% and 4%, respectively) whereas the two non-nucleoside transcriptase inhibitors used in this study, EFV and RPV, have high protein binding values (99.5–99.8%, 99.7%, respectively). Interestingly, EFV has low protein binding in the cerebrospinal fluid, thereby allowing more unbound EFV for tissue distribution.<sup>44,56</sup> All the antiretrovirals used in this *in vivo* study are low-molecular-weight compounds. Lipophilicity is an important factor of drug distribution into brain tissue across the blood brain barrier. Lipophilicity of a drug is predicted by its  $\log P$  value which represents the octanol/water partition coefficient for its neutral form. In general, drugs that have very low  $\log P$  values will not diffuse across the BBB, thereby not facilitating distribution into brain tissue. The predicted  $\log P$  values of TFV, FTC, EFV, and RPV are  $-1.74$ ,  $-0.65$ ,  $4.15$ , and  $4.64$ . TFV and FTC are more hydrophilic and have limited penetration into brain. In contrast, EFV has a high  $\log P$  value indicating higher lipophilicity, thereby allowing high cellular permeability into brain.<sup>57</sup> In addition, since these compounds contain ionizable functional groups, we calculated  $\log D$  (the octanol–water distribution coefficient at a defined pH) values at pH 7. The  $\log D$  values of FTC, TFV, EFV, and RPV at pH 7 are  $-0.9$ ,  $-3.48$ ,  $4.46$ , and  $5.47$ , respectively. Taken together, the degree of protein binding and affinity for lipophilic environment favor EFV distribution in brain. The calculated

TEC values of TFV, FTC, EFV, and RPV in different tissue types provide an approximation of potential ion suppression effects.

In summary, we employed a MALDI MSI strategy to determine the spatial distribution of TFV, FTC, EFV, and RPV following oral *in vivo* dosing. Elucidation of drug distributions as described here would not have been possible using traditional liquid chromatography–mass spectrometry approaches. Remarkably, the results obtained from this proof-of-concept study will increase our understanding of distributions of TFV, FTC, EFV, and RPV in tissues including HIV reservoirs and organs that are associated with drug-induced toxicity. Importantly, the data generated from our MALDI MSI approach can be used to validate physiologically based pharmacokinetic (PBPK)-model-based predictions of tissue drug distributions. Future work is required to determine the quantitative comparisons of drug concentrations in tissues as well as the factors that drive the heterogeneity of TFV, FTC, EFV, and RPV distribution.

## AUTHOR INFORMATION

### Corresponding Author

**Namandjé N. Bumpus** – Department of Medicine, Division of Clinical Pharmacology and Department of Pharmacology and Molecular Sciences, The Johns Hopkins University School of Medicine, Baltimore, Maryland 21205, United States; Phone: +1 410 955 0562; Email: [nbumpus1@jhmi.edu](mailto:nbumpus1@jhmi.edu)

### Authors

**Herana Kamal Seneviratne** – Department of Medicine, Division of Clinical Pharmacology, The Johns Hopkins University School of Medicine, Baltimore, Maryland 21205, United States; [orcid.org/0000-0002-7221-7060](https://orcid.org/0000-0002-7221-7060)

**Allyson N. Hamlin** – Department of Medicine, Division of Clinical Pharmacology, The Johns Hopkins University School of Medicine, Baltimore, Maryland 21205, United States

**Carley J. S. Heck** – Department of Pharmacology and Molecular Sciences, The Johns Hopkins University School of Medicine, Baltimore, Maryland 21205, United States; [orcid.org/0000-0002-6842-3670](https://orcid.org/0000-0002-6842-3670)

Complete contact information is available at: <https://pubs.acs.org/10.1021/acspsci.0c00015>

### Author Contributions

H.K.S., A.N.H., and C.J.S.H. conducted experiments, while all authors participated in research design and data analysis. The manuscript was written through contributions of all authors. All authors have given approval to the final version of the manuscript.

### Notes

The authors declare no competing financial interest.

## ACKNOWLEDGMENTS

This research was funded by the National Institutes of Health [Grants U19AI11327, UM1 AI068613, and R01AI128781].

## ABBREVIATIONS

FTC, emtricitabine; TFV, tenofovir; EFV, efavirenz; RPV, rilpivirine; EFV–OH, hydroxylated EFV; RPV–OH, hydroxylated RPV; HIV, human immunodeficiency virus; TEC, tissue extinction coefficient; MALDI MSI, matrix-assisted laser

desorption/ionization mass spectrometry imaging; CHCA,  $\alpha$ -cyano-4-hydroxycinnamic acid

## REFERENCES

- (1) Saravolatz, L. D., and Saag, M. S. (2006) Emtricitabine, a new antiretroviral agent with activity against HIV and hepatitis B virus. *Clin. Infect. Dis.* 42, 126–131.
- (2) Bang, L. M., and Scott, L. J. (2003) Emtricitabine: an antiretroviral agent for HIV infection. *Drugs* 63, 2413–2424. (see discussion on pp 2425–2416).
- (3) Plosker, G. L. (2013) Emtricitabine/tenofovir disoproxil fumarate: a review of its use in HIV-1 pre-exposure prophylaxis. *Drugs* 73, 279–291.
- (4) Rakhmanina, N. Y., and van den Anker, J. N. (2010) Efavirenz in the therapy of HIV infection. *Expert Opin. Drug Metab. Toxicol.* 6, 95–103.
- (5) Schrijvers, R., Desimmie, B. A., and Debyser, Z. (2011) Rilpivirine: a step forward in tailored HIV treatment. *Lancet* 378, 201–203.
- (6) Cooper, R. D., Wiebe, N., Smith, N., Keiser, P., Naicker, S., and Tonelli, M. (2010) Systematic review and meta-analysis: renal safety of tenofovir disoproxil fumarate in HIV-infected patients. *Clin. Infect. Dis.* 51, 496–505.
- (7) Fernandez-Fernandez, B., Montoya-Ferrer, A., Sanz, A. B., Sanchez-Niño, M. D., Izquierdo, M. C., Poveda, J., Sainz-Prestel, V., Ortiz-Martín, N., Parra-Rodríguez, A., Selgas, R., Ruiz-Ortega, M., Egido, J., and Ortiz, A. (2011) Tenofovir nephrotoxicity: 2011 update. *AIDS Res. Treat.* 2011, 354908.
- (8) Marzolini, C., Telenti, A., Decosterd, L. A., Greub, G., Biollaz, J., and Buclin, T. (2001) Efavirenz plasma levels can predict treatment failure and central nervous system side effects in HIV-1-infected patients. *AIDS* 15, 71–75.
- (9) Declodt, E. H., and Maartens, G. (2013) Neuronal toxicity of efavirenz: a systematic review. *Expert Opin. Drug Saf.* 12, 841–846.
- (10) Kenedi, C. A., and Goforth, H. W. (2011) A systematic review of the psychiatric side-effects of efavirenz. *AIDS Behav* 15, 1803–1818.
- (11) Brück, S., Witte, S., Brust, J., Schuster, D., Mosthaf, F., Procaccianti, M., Rump, J. A., Klinker, H., Petzold, D., and Hartmann, M. (2008) Hepatotoxicity in patients prescribed efavirenz or nevirapine. *Eur. J. Med. Res.* 13, 343–348.
- (12) Kontorinis, N., and Dieterich, D. T. (2003) Toxicity of non-nucleoside analogue reverse transcriptase inhibitors. *Semin. Liver Dis.* 23, 173–182.
- (13) Ogburn, E. T., Jones, D. R., Masters, A. R., Xu, C., Guo, Y., and Desta, Z. (2010) Efavirenz primary and secondary metabolism in vitro and in vivo: identification of novel metabolic pathways and cytochrome P450 2A6 as the principal catalyst of efavirenz 7-hydroxylation. *Drug Metab. Dispos.* 38, 1218–1229.
- (14) Lade, J. M., Avery, L. B., and Bumpus, N. N. (2013) Human biotransformation of the nonnucleoside reverse transcriptase inhibitor rilpivirine and a cross-species metabolism comparison. *Antimicrob. Agents Chemother.* 57, 5067–5079.
- (15) Bumpus, N. N. (2011) Efavirenz and 8-hydroxyefavirenz induce cell death via a JNK- and BimEL-dependent mechanism in primary human hepatocytes. *Toxicol. Appl. Pharmacol.* 257, 227–234.
- (16) Tovar-y-Romo, L. B., Bumpus, N. N., Pomerantz, D., Avery, L. B., Sacktor, N., McArthur, J. C., and Haughey, N. J. (2012) Dendritic spine injury induced by the 8-hydroxy metabolite of efavirenz. *J. Pharmacol. Exp. Ther.* 343, 696–703.
- (17) Palmer, S., Josefsson, L., and Coffin, J. M. (2011) HIV reservoirs and the possibility of a cure for HIV infection. *J. Intern. Med.* 270, 550–560.
- (18) Wong, J. K., and Yukl, S. A. (2016) Tissue reservoirs of HIV. *Curr. Opin. HIV AIDS* 11, 362–370.
- (19) Marban, C., Forouzanfar, F., Ait-Ammar, A., Fahmi, F., El Mekdad, H., Daouad, F., Rohr, O., and Schwartz, C. (2016) Targeting the Brain Reservoirs: Toward an HIV Cure. *Front. Immunol.* 7, 397.
- (20) Nolan, D. J., Rose, R., Rodriguez, P. H., Salemi, M., Singer, E. J., Lamers, S. L., and McGrath, M. S. (2018) The Spleen Is an HIV-1 Sanctuary During Combined Antiretroviral Therapy. *AIDS Res. Hum. Retroviruses* 34, 123–125.
- (21) Fletcher, C. V., Staskus, K., Wietgreffe, S. W., Rothenberger, M., Reilly, C., Chipman, J. G., Beilman, G. J., Khoruts, A., Thorkelson, A., Schmidt, T. E., Anderson, J., Perkey, K., Stevenson, M., Perelson, A. S., Douek, D. C., Haase, A. T., and Schacker, T. W. (2014) Persistent HIV-1 replication is associated with lower antiretroviral drug concentrations in lymphatic tissues. *Proc. Natl. Acad. Sci. U. S. A.* 111, 2307–2312.
- (22) Lee, M. S., and Kerns, E. H. (1999) LC/MS applications in drug development. *Mass Spectrom. Rev.* 18, 187–279.
- (23) Mouton, J. W., Theuretzbacher, U., Craig, W. A., Tulkens, P. M., Derendorf, H., and Cars, O. (2007) Tissue concentrations: do we ever learn? *J. Antimicrob. Chemother.* 61, 235–237.
- (24) Norris, J. L., and Caprioli, R. M. (2013) Analysis of tissue specimens by matrix-assisted laser desorption/ionization imaging mass spectrometry in biological and clinical research. *Chem. Rev.* 113, 2309–2342.
- (25) Angel, P. M., and Caprioli, R. M. (2013) Matrix-assisted laser desorption ionization imaging mass spectrometry: in situ molecular mapping. *Biochemistry* 52, 3818–3828.
- (26) Buck, A., and Walch, A. (2014) In situ drug and metabolite analysis [corrected] in biological and clinical research by MALDI MS imaging. *Bioanalysis* 6, 1241–1253.
- (27) Römpf, A., Guenther, S., Takats, Z., and Spengler, B. (2011) Mass spectrometry imaging with high resolution in mass and space (HR(2) MSI) for reliable investigation of drug compound distributions on the cellular level. *Anal. Bioanal. Chem.* 401, 65–73.
- (28) Seneviratne, H. K., Hendrix, C. W., Fuchs, E. J., and Bumpus, N. N. (2018) MALDI Mass Spectrometry Imaging Reveals Heterogeneous Distribution of Tenofovir and Tenofovir Diphosphate in Colorectal Tissue of Subjects Receiving a Tenofovir-Containing Enema. *J. Pharmacol. Exp. Ther.* 367, 40–48.
- (29) Tetko, I. V., Gasteiger, J., Todeschini, R., Mauri, A., Livingstone, D., Ertl, P., Palyulin, V. A., Radchenko, E. V., Zefirov, N. S., Makarenko, A. S., Tanchuk, V. Y., and Prokopenko, V. V. (2005) Virtual computational chemistry laboratory—design and description. *J. Comput.-Aided Mol. Des.* 19, 453–463.
- (30) Echenique, I. A., and Rich, J. D. (2013) EFV/FTC/TDF-associated hepatotoxicity: a case report and review. *AIDS Patient Care STDS* 27, 493–497.
- (31) Rivero, A., Mira, J. A., and Pineda, J. A. (2007) Liver toxicity induced by non-nucleoside reverse transcriptase inhibitors. *J. Antimicrob. Chemother.* 59, 342–346.
- (32) Patil, R., Ona, M. A., Papafragkakis, H., Carey, J., Moshenyat, Y., Alhaddad, A., and Anand, S. (2015) Acute Liver Toxicity due to Efavirenz/Emtricitabine/Tenofovir. *Case Reports Hepatol* 2015, 280353.
- (33) Lattuada, E., Lanzafame, M., Carolo, G., Gottardi, M., Concia, E., and Vento, S. (2008) Does tenofovir increase efavirenz hepatotoxicity? *AIDS* 22, 995.
- (34) Stephan, C., Dauer, B., Khaykin, P., Stuermer, M., Gute, P., Klauke, S., and Staszewski, S. (2009) Quadruple nucleos(t)ide reverse transcriptase inhibitors-only regimen of tenofovir plus zidovudine/lamivudine/abacavir in heavily pre-treated HIV-1 infected patients: salvage therapy or backbone only? *Curr. HIV Res.* 7, 320–326.
- (35) Molina, J. M., Cahn, P., Grinsztejn, B., Lazzarin, A., Mills, A., Saag, M., Supparatpinyo, K., Walmsley, S., Crauwels, H., Rimsky, L. T., Van Veggel, S., and Boven, K. (2011) Rilpivirine versus efavirenz with tenofovir and emtricitabine in treatment-naive adults infected with HIV-1 (ECHO): a phase 3 randomised double-blind active-controlled trial. *Lancet* 378, 238–246.
- (36) Mutlib, A. E., Chen, H., Nemeth, G. A., Markwalder, J. A., Seitz, S. P., Gan, L. S., and Christ, D. D. (1999) Identification and characterization of efavirenz metabolites by liquid chromatography/mass spectrometry and high field NMR: species differences in the metabolism of efavirenz. *Drug Metab. Dispos.* 27, 1319–1333.

- (37) Ward, B. A., Gorski, J. C., Jones, D. R., Hall, S. D., Flockhart, D. A., and Desta, Z. (2003) The cytochrome P450 2B6 (CYP2B6) is the main catalyst of efavirenz primary and secondary metabolism: implication for HIV/AIDS therapy and utility of efavirenz as a substrate marker of CYP2B6 catalytic activity. *J. Pharmacol. Exp. Ther.* 306, 287–300.
- (38) Heck, C. J. S., Hamlin, A. N., and Bumpus, N. N. (2019) Efavirenz and Efavirenz-like Compounds Activate Human, Murine, and Macaque Hepatic IRE1  $\alpha$ -XBP1. *Mol. Pharmacol.* 95, 183.
- (39) Nelson, D. R., Zeldin, D. C., Hoffman, S. M., Maltais, L. J., Wain, H. M., and Nebert, D. W. (2004) Comparison of cytochrome P450 (CYP) genes from the mouse and human genomes, including nomenclature recommendations for genes, pseudogenes and alternative-splice variants. *Pharmacogenetics* 14, 1–18.
- (40) Sakuma, T., Takai, M., Endo, Y., Kuroiwa, M., Ohara, A., Jarukamjorn, K., Honma, R., and Nemoto, N. (2000) A novel female-specific member of the CYP3A gene subfamily in the mouse liver. *Arch. Biochem. Biophys.* 377, 153–162.
- (41) Sakuma, T., Endo, Y., Mashino, M., Kuroiwa, M., Ohara, A., Jarukamjorn, K., and Nemoto, N. (2002) Regulation of the expression of two female-predominant CYP3A mRNAs (CYP3A41 and CYP3A44) in mouse liver by sex and growth hormones. *Arch. Biochem. Biophys.* 404, 234–242.
- (42) Aouri, M., Barcelo, C., Ternon, B., Cavassini, M., Anagnostopoulos, A., Yerly, S., Hugues, H., Vernazza, P., Günthard, H. F., Buclin, T., Telenti, A., Rotger, M., and Decosterd, L. A. (2016) In Vivo Profiling and Distribution of Known and Novel Phase I and Phase II Metabolites of Efavirenz in Plasma, Urine, and Cerebrospinal Fluid. *Drug Metab. Dispos.* 44, 151–161.
- (43) Leutscher, P. D., Stecher, C., Storgaard, M., and Larsen, C. S. (2013) Discontinuation of efavirenz therapy in HIV patients due to neuropsychiatric adverse effects. *Scand. J. Infect. Dis.* 45, 645–651.
- (44) Curley, P., Rajoli, R. K., Moss, D. M., Liptrott, N. J., Letendre, S., Owen, A., and Siccardi, M. (2017) Efavirenz Is Predicted To Accumulate in Brain Tissue: an In Silico, In Vitro, and In Vivo Investigation. *Antimicrob. Agents Chemother.* 61, e01841-16.
- (45) Thompson, C. G., Bokhart, M. T., Sykes, C., Adamson, L., Fedoriw, Y., Luciw, P. A., Muddiman, D. C., Kashuba, A. D., and Rosen, E. P. (2015) Mass spectrometry imaging reveals heterogeneous efavirenz distribution within putative HIV reservoirs. *Antimicrob. Agents Chemother.* 59, 2944–2948.
- (46) Bertrand, L., Velichkovska, M., and Toborek, M. (2019) Cerebral Vascular Toxicity of Antiretroviral Therapy. *J. Neuroimmune Pharmacol.* DOI: 10.1007/s11481-019-09858-x.
- (47) Bertrand, L., Dygert, L., and Toborek, M. (2016) Antiretroviral Treatment with Efavirenz Disrupts the Blood-Brain Barrier Integrity and Increases Stroke Severity. *Sci. Rep.* 6, 39738.
- (48) Di Mascio, M., Srinivasula, S., Bhattacharjee, A., Cheng, L., Martiniova, L., Herscovitch, P., Lertora, J., and Kiesewetter, D. (2009) Antiretroviral tissue kinetics: in vivo imaging using positron emission tomography. *Antimicrob. Agents Chemother.* 53, 4086–4095.
- (49) Verhelst, D., Monge, M., Meynard, J. L., Fouqueray, B., Mougnot, B., Girard, P. M., Ronco, P., and Rossert, J. (2002) Fanconi syndrome and renal failure induced by tenofovir: a first case report. *Am. J. Kidney Dis.* 40, 1331–1333.
- (50) Rifkin, B. S., and Perazella, M. A. (2004) Tenofovir-associated nephrotoxicity: Fanconi syndrome and renal failure. *Am. J. Med.* 117, 282–284.
- (51) Tourret, J., Deray, G., and Isnard-Bagnis, C. (2013) Tenofovir effect on the kidneys of HIV-infected patients: a double-edged sword? *J. Am. Soc. Nephrol.* 24, 1519–1527.
- (52) Cihlar, T., Ho, E. S., Lin, D. C., and Mulato, A. S. (2001) Human renal organic anion transporter 1 (hOAT1) and its role in the nephrotoxicity of antiviral nucleotide analogs. *Nucleosides, Nucleotides Nucleic Acids* 20, 641–648.
- (53) Imaoka, T., Kusuhara, H., Adachi, M., Schuetz, J. D., Takeuchi, K., and Sugiyama, Y. (2007) Functional involvement of multidrug resistance-associated protein 4 (MRP4/ABCC4) in the renal elimination of the antiviral drugs adefovir and tenofovir. *Mol. Pharmacol.* 71, 619–627.
- (54) Kohler, J. J., Hosseini, S. H., Green, E., Abuin, A., Ludaway, T., Russ, R., Santoianni, R., and Lewis, W. (2011) Tenofovir renal proximal tubular toxicity is regulated by OAT1 and MRP4 transporters. *Lab. Invest.* 91, 852–858.
- (55) Desai, M., Joyce, V., Bendavid, E., Olshen, R. A., Hlatky, M., Chow, A., Holodniy, M., Barnett, P., and Owens, D. K. (2015) Risk of cardiovascular events associated with current exposure to HIV antiretroviral therapies in a US veteran population. *Clin. Infect. Dis.* 61, 445–452.
- (56) Avery, L. B., Sacktor, N., McArthur, J. C., and Hendrix, C. W. (2013) Protein-free efavirenz concentrations in cerebrospinal fluid and blood plasma are equivalent: applying the law of mass action to predict protein-free drug concentration. *Antimicrob. Agents Chemother.* 57, 1409–1414.
- (57) Siccardi, M., Almond, L., Schipani, A., Csajka, C., Marzolini, C., Wyen, C., Brockmeyer, N. H., Boffito, M., Owen, A., and Back, D. (2012) Pharmacokinetic and pharmacodynamic analysis of efavirenz dose reduction using an in vitro-in vivo extrapolation model. *Clin. Pharmacol. Ther.* 92, 494–502.